METALLURGY

Enhanced thermal stability of nanograined metals below a critical grain size

X. Zhou,[1,2] X. Y. Li,[1]* K. Lu[1]*

The limitation of nanograined materials is their strong tendency to coarsen at elevated temperatures. As grain size decreases into the nanoscale, grain coarsening occurs at much lower temperatures, as low as ambient temperatures for some metals. We discovered that nanometer-sized grains in pure copper and nickel produced from plastic deformation at low temperatures exhibit notable thermal stability below a critical grain size. The instability temperature rises substantially at smaller grain sizes, and the nanograins remain stable even above the recrystallization temperatures of coarse grains. The inherent thermal stability of nanograins originates from an autonomous grain boundary evolution to low-energy states due to activation of partial dislocations in plastic deformation.

Refining grains of metals into the nanometer scale may greatly enhance their strength and hardness (*1*). But the introduced high density of grain boundaries (GBs) provides a strong driving force for grain coarsening accompanied by property degradation. The instability temperature, which marks the onset of grain coarsening, decreases substantially for nanometer-sized grains in metals (*1*–*3*). In some nanograined metals, such as Cu, coarsening occurs even at ambient temperatures (*1*, *4*). The inherent thermal instability is an "Achilles' heel" of nanograined materials and hinders technological applications at elevated temperatures. The temperature response also complicates the processing of nanograined metals for further structure refinement and property enhancements (*1*).

Grain coarsening in polycrystals is basically a GB migration process, which can be inhibited by various alloy methods. Coarsening kinetics can be suppressed by pinning GBs with a second-phase drag, a solute or impurity drag, or by chemical ordering (*5*–*8*). Lowering GB energy by solute segregation may reduce the thermodynamic driving force for coarsening and hence stabilize the nanograins as well, as observed in FeP, Ni-P, and Pd-Zr systems (*9*–*11*). But these alloy-based approaches may unavoidably influence, and often deteriorate, mechanical, physical, or chemical properties of nanograined materials. Stabilizing nanograined structures in pure metals without alloying is technically challenging.

Recent experimental results showed elevated thermal stabilities of nanolaminated structures in several pure metals with low-energy interfaces, such as twin boundaries or low-angle boundaries (*12*, *13*), relative to nanograined structures with conventional high-angle GBs. Apparently, reduced interfacial excess energy is effective to stabilize nanostructures in pure metals (*1*). Nevertheless, generating three-dimensional nanograins in pure metals with every GB in a low-energy state is practically very difficult. We discovered an autonomous structural evolution in GBs toward low-energy states in pure Cu and Ni as the grain sizes were reduced below a critical value by plastic deformation. This evolution led to notable thermal stability in nanograins, for which the apparent instability temperature was even higher than that for coarse grains.

We processed coarse-grained oxygen-free Cu bar specimens with a purity of 99.97% by using a surface mechanical grinding treatment (SMGT) in liquid nitrogen to generate a gradient nanograined surface layer (*14*) (table S1). After the treatment, randomly oriented grains with an average transversal size of ~40 ± 2 nm and an aspect ratio of 1.7 were formed in the topmost surface layer (Fig. 1, A and B). Using longitude-sectional transmission electron microscopy (TEM) measurements, we found that the transversal grain sizes increased gradually with increasing depth, to about 70 nm at a 20-μm depth and 200 nm at an ~150-μm depth. We observed deformed coarse-grained structures adherent on the deformation-free core in the depth span of 150 to 500 μm.

We found weak {111}<110> texture in the surface layer of the as-prepared SMGT Cu sample with the use of electron diffraction analysis under TEM and electron backscattered diffraction (EBSD). The fraction of material with this texture changed slightly from 37.3% at the topmost surface level to 31.5% at a 40-μm depth (*14*) (fig. S5). We examined possible processing-induced contamination in the surface layer with the use of TEM–energy-dispersive spectroscopy and electron energy loss spectroscopy. The composition remained constant with increasing depth, and we did not detect impurities such as carbon and oxygen deeper than 0.5 μm from the processed surface in Cu (*14*) (fig. S4). The compositional stability resulted from performing the SMGT process in liquid nitrogen, which suppressed the atomic diffusion of elements. We removed the measurement data for the topmost 1-μm-thick layer from our analysis to avoid any potential contamination and surface effects.

We examined the grain size effects on thermal stability with the use of scanning electron microscopy (SEM) observations of the gradient nanograined specimens annealed at various temperatures for 30 min (Fig. 1A and fig. S1) (*14*). As annealing temperatures exceeded 373 K, sporadic coarsened grains began to appear in the subsurface layer in a depth span of 20 to 50 μm, where the original grains were 70 to 110 nm in size. At higher temperatures, coarsening became more evident and the coarsening layer thickened. At 453 K, the upper front of the coarsening layer migrated slightly upward and the lower front migrated downward to ~120 μm deep, where the initial grain sizes were ~175 nm. The grain size and nanohardness profiles we measured along increasing depths for the annealed samples showed an obvious softening corresponding to the coarsening in the subsurface layer (Fig. 1F). The higher the annealing temperature, the lesser the hardness and the larger the depth span of the coarsening layer, consistent with SEM observations.

Coarsening should start with the topmost, smallest grains instead of the subsurface layers. We were surprised to find coarsening begin in a different part of our sample. More notably, we did not detect any grain coarsening under SEM in the top 20-μm-thick surface layer that we annealed below 453 K (Fig. 1, A and D). We observed no obvious change in either the morphology or the size of the nanograins after annealing (the average transversal size was 43 ± 2 nm after annealing at 433 K) (Fig. 1C) with the use of TEM characterization. Under the same annealing conditions, the submicrometer-sized grains in deep layers coarsened into micrometer-sized grains. The hardness of the nanograined top layer we measured remained unchanged after annealing, verifying the TEM and SEM results. The nanograins were stable as annealed at 433 K even for 12 hours (*14*) (fig. S3). Clearly, the degree of thermal stability of the nanograins in the top layer was higher, rather than lower, than that of the submicrometer-sized grains.

As annealing temperatures exceeded 453 K, large grains appeared in the top surface layer (Fig. 1, A and E), most of them elongated, more than 10 μm long in parallel to the surface, and a few micrometers thick. These large grains were recrystallization products of the nanograins, but their morphologies were distinct from those of the coarsened grains underneath. Increasing the annealing temperature caused more recrystallized grains to form. These grains were embedded in the nanograins and were attached to the underneath coarsened grains, located in the interior of the nanograined layer, or found in the topmost surface layer (Fig. 1, A and E). We frequently

[1]Shenyang National Laboratory for Materials Science, Institute of Metal Research, Chinese Academy of Sciences, 72 Wenhua Road, Shenyang 110016, China. [2]School of Materials Science and Engineering, University of Science and Technology of China, Hefei 230026, China.
*Corresponding author. Email: xyli@imr.ac.cn (X.Y.L.); lu@imr.ac.cn (K.L.)

observed nanograined layers sandwiched with recrystallized grains. We were surprised that some nanograins remained stable even after annealing at 623 K (*14*), about 230 K higher than the coarsening temperature for the submicrometer-sized grains in the same sample. We found a general trend in that the smaller grains closer to the surface were more resistant to recrystallization. As the annealing temperature exceeded 623 K, no nanograins survived and the top surface layer fully recrystallized.

Several lines of observational evidence indicated that the nanograins in the top surface layer were more thermally stable than the larger grains. This relationship differs fundamentally from the traditional view of the "smaller less-stable" trend with regard to thermal stability. This difference is not from surface contaminations or texture effects, as we found no change in chemical composition and texture across the grain size regime (*14*). Recrystallization of nanograins at the topmost surface level before those in the interior is an indicator of negligible contamination at the processed surface. For further verification, we used the same SMGT process but with lower strain rates and a higher temperature (173 K) to prepare submicrometer-sized grains in the top surface layer (Fig. 2). Annealing this gradient submicrometer-grained sample above 433 K, we found grain coarsening onset at the top surface with the smallest grains and in the subsurface layer (Fig. 2B). At higher annealing temperatures, the coarsening continued throughout a surface layer that was more than 100 μm thick (Fig. 2C). These results support our discovery that the marked thermal stability of the surface nanograins is a grain size effect rather than a result of processing-induced contamination.

We annealed a number of individual specimens by heating them directly to preset temperatures and holding at those temperatures for 30 min (*14*) (fig. S1) to determine the grain-coarsening temperature as a function of initial grain size in Cu samples (Fig. 3A) (*15*–*21*). We found that for grain sizes above 70 nm, the coarsening temperature drops with decreasing size, in agreement with the reported trend for nanograined Cu processed from different plastic deformation routes. Grains below 70 nm exhibit distinct stability. Smaller nanograins become more stable, and their instability temperature rises up to $0.45T_m$ (T_m is the equilibrium melting point), which is even higher than that of the recrystallization temperatures of coarse-grained Cu (usually below $0.4T_m$). The instability temperature for 40-nm grains in the topmost surface layer (623 K) is about 290 K higher than that for Cu grains with comparable sizes prepared from inert gas condensation (~333 K), which falls in line with the conventional trend.

We performed the same experiments with gradient nanograined Ni samples (99.5% purity) prepared with the use of SMGT. As we observed in Cu, nanograins in the top surface layer exhibited much higher stability against annealing than the submicrometer-sized grains in the subsurface layer (Fig. 4, A and B). The sizes and morphologies of the nanograins remained stable even after annealing at 873 K (Fig. 4, C to E). Under the same annealing conditions, micrometer-sized grains were formed in the subsurface layer with initial grain sizes larger than 90 nm. The variation of grain coarsening temperature with initial grain size in Ni was similar to that in Cu. The instability temperature of nanograins in Ni can be as high as 1173 K (~$0.68T_m$) (*14*) (fig. S2), which is much higher than the recrystallization temperature of coarse-grained Ni (Fig. 4F) (*13*, *22*, *23*).

Generally, the driving force for recrystallization and coarsening of the nanograins is stored energy in the forms of dislocations and GBs. We measured this energy by differential scanning calorimetry (DSC) (*14*). We cut foil specimens with nanograins and submicrometer-sized grains at different depths from the as-prepared Cu sample. Upon heating, an exothermic peak due to

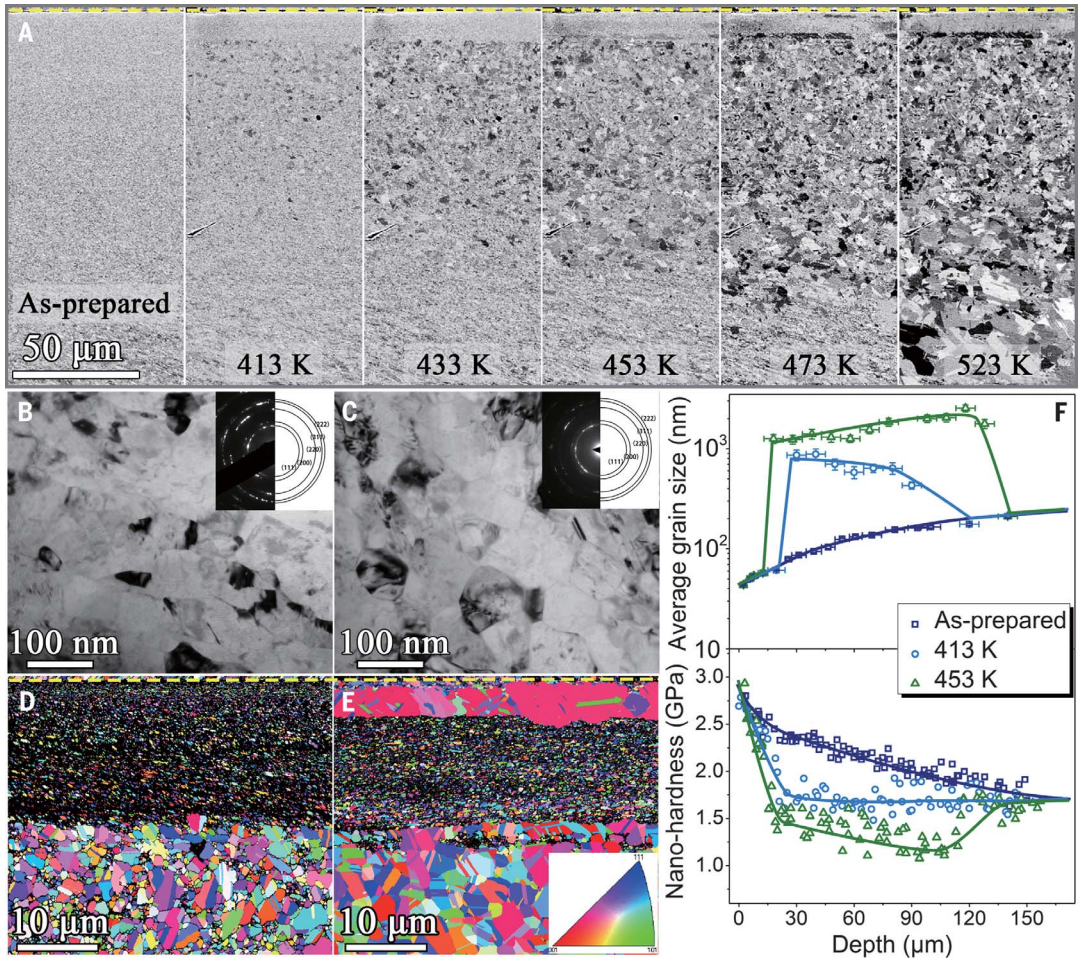

Fig. 1. Annealing-induced structure changes in the gradient nanograined structure in pure Cu. (**A**) Cross-sectional SEM images of the as-prepared gradient nanograined Cu sample (left) and samples after ex situ annealing at various temperatures (as indicated) for 30 min. Dotted lines represent the treated surface. Cross-sectional bright-field TEM images with selected area electron diffraction patterns (insets) for the nanograins at a depth of 2 μm from the surface in the as-prepared sample (**B**) and a sample annealed at 433 K for 30 min (**C**). Typical cross-sectional EBSD images of the top surface layer in the Cu samples annealed at 433 K (**D**) and 473 K (**E**) for 30 min. (**F**) Variations of average grain size and nanohardness along increasing depths from the surface in the as-prepared and the as-annealed Cu samples treated at 413 and 453 K for 30 min. Error bars indicate the variation range of measured statistic grain sizes within a depth span.

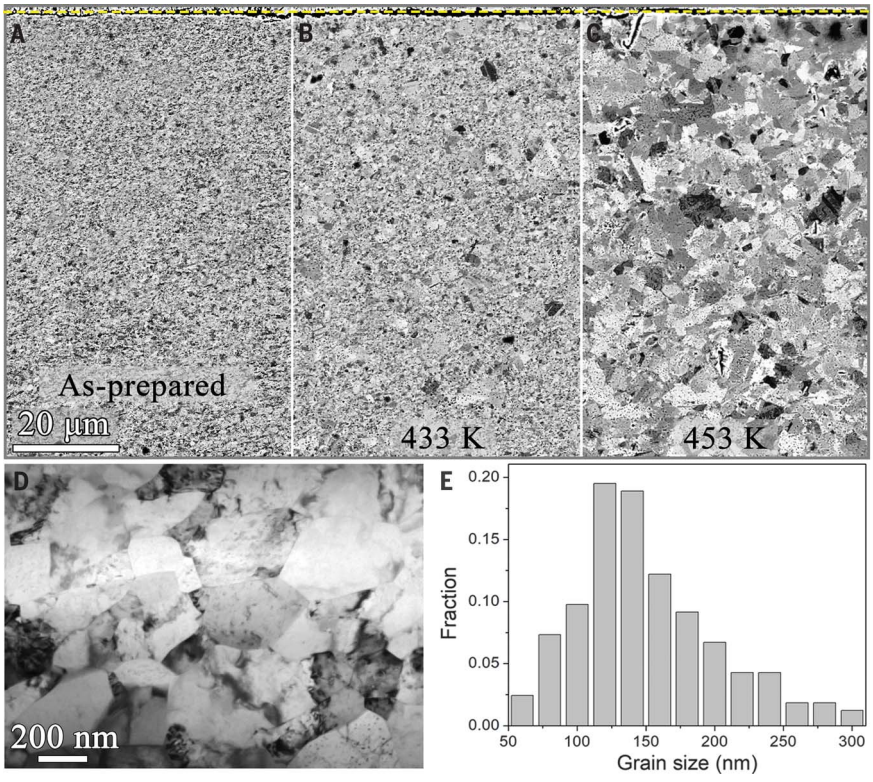

Fig. 2. Annealing-induced coarsening of submicrometer grains in the top surface layer in Cu. Cross-sectional SEM images of the as-prepared gradient submicrometer-grained Cu sample (**A**) and samples after annealing at 433 K (**B**) and 453 K (**C**) for 30 min. Dotted lines represent the treated surface. (**D**) A bright-field TEM image of the top surface layer. (**E**) Corresponding grain size distribution, with an average size of 140 nm.

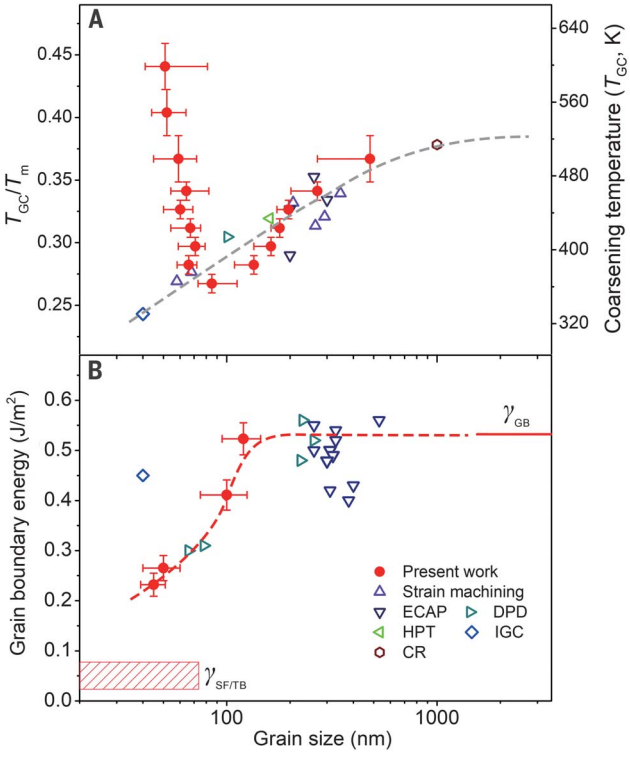

Fig. 3. Grain size dependence of instability temperature and GB energy in Cu. Measured grain coarsening (instability) temperature (T_{GC}) (**A**) and GB excess energy (**B**) as a function of average grain size in Cu. Literature data for Cu processed with different techniques [strain machining (*15*), equal-channel angle pressing (ECAP) (*16*, *17*, *24*, *25*), dynamic plastic deformation (DPD) (*18*), high-pressure torsion (HPT) (*19*), cold rolling (CR) (*20*), and inert gas condensation (IGC) (*21*)] are included. Conventional GB energies (γ_{GB}) and energies for stacking faults and twin boundaries ($\gamma_{SF/TB}$) of Cu are indicated. Error bars in (A) indicate the variation range of measured instability temperatures within a grain size span. Error bars in (B) indicate the variation range of measured GB energies within the grain size span.

recrystallization and grain coarsening of the nanostructures appeared. With the measured enthalpy release and grain size changes, specific GB excess energy was determined to be ~0.52 ± 0.03 J/m^2 (minor contributions of other defects were ignored) for an average grain size of 125 nm. This value is consistent with the conventional GB energy for Cu (*21*, *24*, *25*) and for submicrometer-grained Cu produced from plastic deformation. For grain sizes of ~50 nm, we obtained GB energies of 0.23 to 0.27 J/m^2, only half of conventional GB energy but consistent with that in nanograined Cu prepared from plastic deformation (*18*). From the available GB energy data for Cu processed with different plastic deformation techniques, we noticed an obvious drop in GB energy as grain sizes decreased below ~100 nm (Fig. 3B). This seems analogous to the observation that more stable interfaces with low excess energy were formed during extreme plastic straining in bimetal nanoscale multilayer films (*26*).

We found a reasonable correlation between the critical grain sizes for the GB energy drop and the thermal stability change (Fig. 3, A and B) when measurement errors in grain size were taken into account. A drop in GB energy means a reduced driving force for recrystallization, consistent with the enhanced thermal stability of nanograins below a critical size. Our measured GB energy for a size of ~50 nm is much lower than that for comparable grain sizes prepared from inert gas condensation (0.45 J/m^2) (*21*) but is in good accord with the difference in thermal stability we observed.

The GB energy drop we observed at small grain sizes may be inferred from the grain refinement mechanism and the GB relaxation process during plastic deformation. Because of the high strain rates and low temperatures, plastic deformation in the top surface layer of the SMGT samples is dominated by the formation of stacking faults and twin boundaries. In terms of the grain refinement mechanism discussed previously in the literature (*27*, *28*), most nanograins were formed from fragmentation or shear banding of the lamellar bundles of nanoscale twins and stacking faults, generating plenty of GBs that are in low-energy configurations, analogous to those in the nanograined Cu produced from dynamic plastic deformation (*18*). TEM observations of the SMGT Ni samples showed that the fraction of grains containing twins or stacking faults in the top surface layer is much higher than that in deep layers (*14*) (fig. S6).

In addition, plastic straining may trigger relaxation of GBs in nanograins so that GB structures transform into a lower energy state via GB dissociation processes (*29*–*31*). Simulations and experimental investigations on a range of tilt GBs in several face-centered cubic metals indicated that dissociation of GBs occurs by emission of stacking faults (*29*). This provides a general mode of GB relaxation, especially in metals with low stacking fault energies, such as Cu. Similar processes are anticipated in high–stacking fault energy metals such as Ni under high shear stress, as in our process. Formation of nanometer-scale

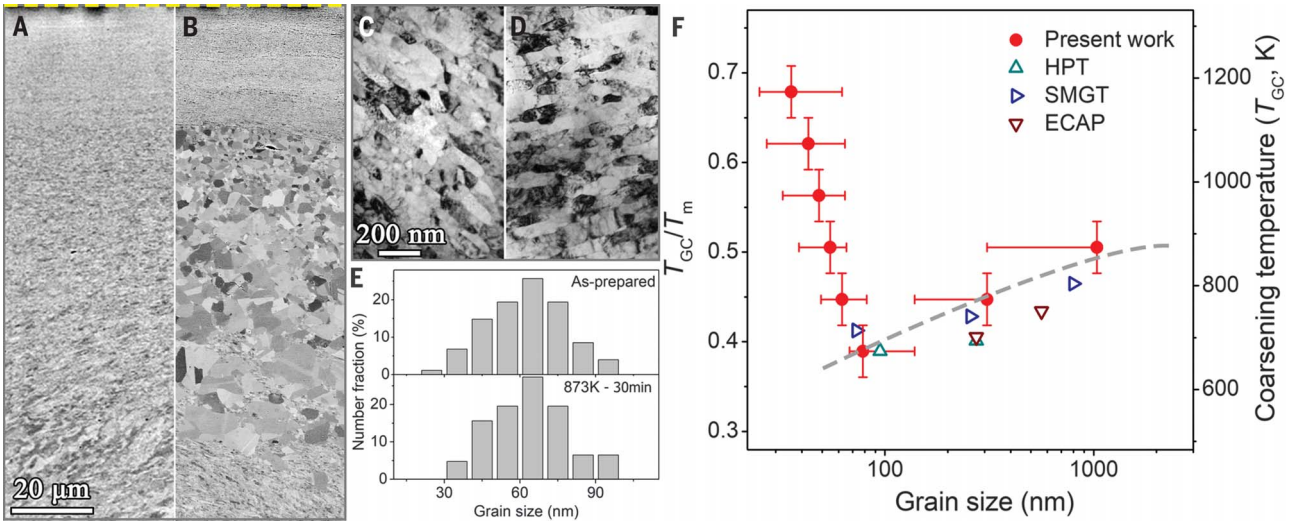

Fig. 4. Annealing-induced structure changes in the gradient nangrained structure in pure Ni. Cross-sectional SEM images of the as-prepared gradient nanograined Ni sample (**A**) and a sample after annealing at 873 K for 30 min (**B**). Dotted lines represent the treated surface. Typical bright-field cross-sectional TEM images of the nanograins (at a depth of ~25 μm from the surface) in the as-prepared state (**C**) and after annealing at 873 K (**D**) and the corresponding grain size distributions (**E**). (**F**) Measured grain coarsening temperature as a function of average grain size in Ni. Literature data for Ni processed with different techniques [HPT (*22*), ECAP (*23*), and SMGT (*13*)] are included. Error bars indicate the variation range of measured instability temperatures within a grain size span.

twins from a GB is also able to lower the GB energy state, as it has been observed that atomic diffusion in Cu is obviously slowed along the GBs adjacent to the triple point where they meet a twin boundary (*32*). Formation of stacking faults or twins from GBs, both with evolving emissions of partial dislocations, may induce GB relaxation to lower energy states and stabilization.

Dislocation activity is grain size dependent. Full dislocation activity may be inhibited at very small grain sizes as partial dislocation activity becomes more favorable. In terms of the Orowan relation (*33*), the resolved shear stress required for expansion of a dislocation loop with a diameter of D is $\tau_{RSS} = \frac{\mu b}{D}$, where μ is the shear modulus and b is the Burgers vector of dislocation. Full dislocation multiplication requires that Frank-Read–type sources have a minimum grain size (D^*) at the yield strength (σ_y) of

$$D^* = \frac{\mu b}{\sigma_y(D^*)/m}$$

where $1/m$ is the average Schmid factor for polycrystals ($m = 3$). In terms of the yield strength of the nanograined Cu, the calculated critical size is D^* = 70 nm [which is very close to that reported by Legros *et al.* (*34*)]. This would mean that as Cu grain sizes become smaller than 70 nm, full dislocation is inhibited and partial dislocation activity becomes dominant in the deformation of most grains, hence enhancing the GB relaxation process. This behavior is exactly what we observed, as both the GB energy drop and the enhanced thermal stability in nanograined Cu appeared around this critical size. As the GB relaxation process is triggered by plastic deformation, it may not happen in the nanograined metals produced from inert gas condensation, which possess high GB energy and hence poor thermal stability (Fig. 3).

The discovery of the marked thermal stability of nanograins in Cu and Ni is important for understanding the nature of GBs at the nanoscale and their response to external thermal and mechanical stimuli. Stabilizing nanograins is also vital for developing stable nanostructured metals and alloys for high-temperature applications.

REFERENCES AND NOTES

1. K. Lu, *Nat. Rev. Mater.* **1**, 16019 (2016).
2. C. C. Koch, R. O. Scattergood, K. A. Darling, J. E. Semones, *J. Mater. Sci.* **43**, 7264–7272 (2008).
3. C. C. Koch, *J. Mater. Sci.* **42**, 1403–1414 (2007).
4. Y. Huang *et al.*, *Mater. Sci. Eng. A* **656**, 55–66 (2016).
5. J. Weissmüller, *Nanostruct. Mater.* **3**, 261–272 (1993).
6. R. Kirchheim, *Acta Mater.* **50**, 413–419 (2002).
7. P. C. Millett, R. P. Selvam, A. Saxena, *Acta Mater.* **55**, 2329–2336 (2007).
8. T. Chookajorn, H. A. Murdoch, C. A. Schuh, *Science* **337**, 951–954 (2012).
9. F. Liu, R. Kirchheim, *J. Cryst. Growth* **264**, 385–391 (2004).
10. K. Boylan, D. Ostrander, U. Erb, G. Palumbo, K. T. Aust, *Scr. Metall. Mater.* **25**, 2711–2716 (1991).
11. B. K. VanLeeuwen, K. A. Darling, C. C. Koch, R. O. Scattergood, B. G. Butler, *Acta Mater.* **58**, 4292–4297 (2010).
12. X. Zhang, A. Misra, *Scr. Mater.* **66**, 860–865 (2012).
13. X. C. Liu, H. W. Zhang, K. Lu, *Science* **342**, 337–340 (2013).
14. See supplementary materials.
15. C. Saldana, A. H. King, S. Chandrasekar, *Acta Mater.* **60**, 4107–4116 (2012).
16. Y. Zhang, J. T. Wang, C. Cheng, J. Q. Liu, *J. Mater. Sci.* **43**, 7326–7330 (2008).
17. N. Lugo, N. Llorca, J. J. Suñol, J. M. Cabrera, *J. Mater. Sci.* **45**, 2264–2273 (2010).
18. Y. Zhang, N. R. Tao, K. Lu, *Acta Mater.* **56**, 2429–2440 (2008).
19. P. Jenei, J. Gubicza, E. Y. Yoon, H. S. Kim, J. L. Lábár, *Compos. Part A Appl. Sci. Manuf.* **51**, 71–79 (2013).
20. Z. N. Mao *et al.*, *Mater. Sci. Eng. A* **674**, 186–192 (2016).
21. A. Kumpmann, B. Günther, H. D. Kunze, *Mater. Sci. Eng. A* **168**, 165–169 (1993).
22. H. W. Zhang, X. Huang, R. Pippan, N. Hansen, *Acta Mater.* **58**, 1698–1707 (2010).
23. S. V. Divinski, G. Reglitz, M. Wegner, M. Peterlechner, G. Wilde, *J. Appl. Phys.* **115**, 113503 (2014).
24. O. F. Higuera-Cobos, J. M. Cabrera, *Mater. Sci. Eng. A* **571**, 103–114 (2013).
25. C. F. Gu, C. H. J. Davies, *Mater. Sci. Eng. A* **527**, 1791–1799 (2010).
26. I. J. Beyerlein *et al.*, *Proc. Natl. Acad. Sci. U.S.A.* **111**, 4386–4390 (2014).
27. K. Wang, N. R. Tao, G. Liu, J. Lu, K. Lu, *Acta Mater.* **54**, 5281–5291 (2006).
28. W. L. Li, N. R. Tao, K. Lu, *Scr. Mater.* **59**, 546–549 (2008).
29. J. D. Rittner, D. N. Seidman, K. L. Merkle, *Phys. Rev. B* **53**, R4241–R4244 (1996).
30. P. M. Derlet, H. Van Swygenhoven, A. Hasnaoui, *Philos. Mag.* **83**, 3569–3575 (2003).
31. R. G. Hoagland, S. M. Valone, *Philos. Mag.* **95**, 112–131 (2015).
32. K. C. Chen, W. W. Wu, C. N. Liao, L. J. Chen, K. N. Tu, *Science* **321**, 1066–1069 (2008).
33. E. Orowan, in *Symposium on Internal Stresses in Metals and Alloys* (Institute of Metals, 1948), p. 451.
34. M. Legros, B. R. Elliott, M. N. Rittner, J. R. Weertman, K. J. Hemker, *Philos. Mag. A* **80**, 1017–1026 (2000).

ACKNOWLEDGMENTS

We thank F. H. Duan for technical assistance with DSC experiments. **Funding:** This work was supported by the Ministry of Science and Technology of China (grants 2012CB932201 and 2017YFA0204401), the National Science Foundation of China (grant 51231006), and the Chinese Academy of Sciences (grant zdyz201701). **Author contributions:** X.Y.L. and K.L. initiated the study; X.Z. and X.Y.L. performed the experiments; X.Z., X.Y.L., and K.L. analyzed the results; and X.Y.L. and K.L. wrote the paper. **Competing interests:** We declare no competing financial interests. **Data and materials availability:** All data are available in the main text or the supplementary materials.

SUPPLEMENTARY MATERIALS

www.sciencemag.org/content/360/6388/526/suppl/DC1
Materials and Methods
Figs. S1 to S6
Table S1

7 December 2017; accepted 26 March 2018
10.1126/science.aar6941

Enhanced thermal stability of nanograined metals below a critical grain size

X. Zhou, X. Y. Li and K. Lu

Science **360** (6388), 526-530.
DOI: 10.1126/science.aar6941

Smaller but more thermally stable

Synthesizing metals with extremely small (nanoscale) grain sizes makes for much stronger materials. However, very small–grained materials start to coarsen at relatively low temperatures, wiping out their most desirable properties. Zhou *et al.* discovered a way to avoid this problem by mechanically grinding copper and nickel at liquid nitrogen temperatures. The processing method creates low-angle grain boundaries between the nanograins, which promotes thermal stability.

Science, this issue p. 526